

NUMERICAL SOLUTION OF THE MODIFIED BESSEL EQUATION

MICHAEL CARLEY*

Abstract. A Green's function based solver for the modified Bessel equation has been developed with the primary motivation of solving the Poisson equation in cylindrical geometries. The method is implemented using a Discrete Hankel Transform and a Green's function based on the modified Bessel functions of the first and second kind. The computation of these Bessel functions has been implemented to avoid scaling problems due to their exponential and singular behavior, allowing the method to be used for large order problems, as would arise in solving the Poisson equation with a dense azimuthal grid. The method has been tested on monotonically decaying and oscillatory inputs, checking for errors due to interpolation and/or aliasing. The error has been found to reach machine precision and to have computational time linearly proportional to the number of nodes.

Key words. ordinary differential equation, modified Bessel function, Poisson equation

AMS subject classifications.

1. Introduction. This paper is motivated by the requirement for a Poisson solver for cylindrical domains. Such a solver is a basic element in solving a range of physical problems and accurate methods have been developed for Cartesian [5] and cylindrical [3] domains. An issue which arises in solving the problem in a cylindrical coordinate system is the singularity which arises at the axis due to the form of the differential operator. A recent paper by Pataki and Greengard [11] introduces a Green's function solver for the Poisson equation, which avoids problems with this singularity, and automatically imposes a radiation boundary condition, by using an integral formulation for the solution.

The method which Pataki and Greengard [11] develop is based on Fourier transforms in the axial and azimuthal coordinate, followed by the solution of a modified Bessel equation in the radial coordinate. They test the accuracy of their method on an axisymmetric problem with monotonic decay in radius, and show its application to an asymmetric problem. A problem which arises in their algorithm is that the integration technique used does not work well for large azimuthal orders, i.e. meshes dense in angle, or for large axial wavenumbers, i.e. meshes dense in the axial coordinate, due to the poor scaling of the modified Bessel functions which appear in the Green's function for the problem.

This motivated an attempt to find a robust method for solving the modified Bessel equation, which would work for large wavenumbers and azimuthal orders. The method developed, which is described in the rest of this paper, is based on the Discrete Hankel Transform (DHT), tabulated integrals, and recursions for the modified Bessel functions.

2. Problem formulation. The Poisson equation in cylindrical coordinates is:

$$u_{rr}(r, \theta, z) + \frac{1}{r}u_r(r, \theta, z) + \frac{1}{r}u_{\theta\theta}(r, \theta, z) + u_{zz}(r, \theta, z) = f(r, \theta, z), \quad (2.1)$$

where (r, θ, z) are cylindrical coordinates, u is the solution and f is some forcing term. With the problem defined on nodes regularly spaced in θ and z , this equation can be solved [11] by using the FFT to Fourier transform u and f in θ and z to yield a set

*Department of Mechanical Engineering, University of Bath, Bath BA2 7AY, United Kingdom (m.j.carley@bath.ac.uk)

of modified Bessel equations:

$$u_{rr}^{(n)}(r, \kappa) + \frac{1}{r}u_r^{(n)}(r, \kappa) - \left(\frac{n^2}{r^2} + \kappa^2\right)u^{(n)}(r, \kappa) = f^{(n)}(r, \kappa), \quad (2.2)$$

where n is the azimuthal order and κ the axial wavenumber, with $u^{(n)}$ and $f^{(n)}$ the Fourier transformed solution and forcing term respectively. After solving Equation 2.2 for each value of n and κ , $u^{(n)}(r, \kappa)$ can be inverse Fourier transformed to yield the solution $u(r, \theta, z)$.

Pataki and Greengard [11] give a method for solving this modified Bessel equation, subject to a radiation boundary condition at some outer radius $r = R$. This is done using the Green's function for the modified Bessel equation with the solution written:

$$u^{(n)}(r, \kappa) = \int_0^R G_n(\kappa, r, s) f(s, \kappa) ds. \quad (2.3)$$

The Green's function G_n is:

$$G_n(\kappa, r, s) = \begin{cases} -sI_n(\kappa r)K_n(\kappa s), & r \leq s; \\ -sK_n(\kappa r)I_n(\kappa s), & r \geq s, \end{cases} \quad (2.4)$$

where $I_n(x)$ and $K_n(x)$ are the modified Bessel functions of the first and second kind respectively. The first of these, I_n , grows exponentially, while K_n decays exponentially, but has $x^{-n} \log x$ behavior at the origin, leading to some numerical problems caused by the scaling of the Green's function. In practice, the solution is computed as:

$$\begin{aligned} u^{(n)}(r, \kappa) = & -\frac{K_n(\kappa r)}{K_n(\kappa R_m)} \int_0^r I_n(\kappa s) K_n(\kappa R_m) f^{(n)}(s) s ds \\ & - I_n(\kappa r) K_n(\kappa R_m) \int_r^R \frac{K_n(\kappa s)}{K_n(\kappa R_m)} f^{(n)}(s) s ds, \end{aligned} \quad (2.5)$$

where the radial domain is divided at radii R_m which are used to set reference values of the modified Bessel functions. The product $I_n(\kappa s)K_n(\kappa R_m)$, and the ratio $K_n(\kappa s)/K_n(\kappa R_m)$, are thus well-scaled avoiding problems in computation, as long as $|\kappa(s - R_m)|$ is not too large. Pataki [10] reports that the integration is performed using a dyadic grid, and that by scaling the modified Bessel functions as they are computed, the method works well for $n \lesssim 40$, corresponding to 80 points in the azimuthal mesh.

For many applications, it is desirable to use a denser mesh than this and so a different approach was sought for the solution of Equation 2.2. The natural transform technique for problems in polar coordinates is the Discrete Hankel Transform (DHT), which expands a function as a series of ordinary Bessel functions $J_m(x)$. For a function $f(r)$, $0 \leq r \leq R$:

$$f(r) \approx \sum_{m=1}^M \hat{f}_m J_m(\alpha_m r) \quad (2.6)$$

where $J_m(\alpha_m R) \equiv 0$ and \hat{f}_m denotes the m coefficient of the expansion of f . If the DHT of $f^{(n)}(r, \kappa)$ is available, the solution of Equation 2.2 can be immediately written:

$$u^{(n)}(r, \kappa) = \sum_{m=1}^M \hat{f}_m \int_0^R J_m(\alpha_m s) G_n(\kappa, r, s) ds. \quad (2.7)$$

The integrals required in Equation 2.7 are given in standard tables [7]:

$$\int_0^r I_n(\kappa s) J_n(\alpha s) s \, ds = [\alpha J_{n+1}(\alpha r) I_n(\kappa r) + \kappa I_{n+1}(\kappa r) J_n(\alpha r)] \frac{r}{\alpha^2 + \kappa^2}, \quad (2.8a)$$

$$\int_0^r K_n(\kappa s) J_n(\alpha s) s \, ds = \left[\left(\frac{\alpha}{\kappa} \right)^n + \alpha r J_{n+1}(\alpha r) K_n(\kappa r) - \kappa r K_{n+1}(\kappa r) J_n(\alpha r) \right] \frac{1}{\alpha^2 + \kappa^2} \quad (2.8b)$$

which gives a solution for the problem in terms of the DHT coefficients $\widehat{f^{(n)}}_m$ and κ . As written, this solution is correct, but not numerically useful, due to the poor scaling of the modified Bessel functions, especially for large values of κ and/or n . It must be rewritten in order to avoid numerical difficulties.

3. Numerical implementation. In order to avoid numerical difficulties caused by poor scaling of the modified Bessel function, Equations 2.8 are rewritten and used to give the convolution of the Green's function with the ordinary Bessel function as:

$$\begin{aligned} \int_0^R G_n(\kappa, r, s) J_n(\alpha s) \, ds = & \\ & - R \frac{I_n(\kappa r) K_n(\kappa R)}{\alpha^2 + \kappa^2} \left[\alpha J_{n+1}(\alpha R) - \kappa J_n(\alpha R) \frac{K_{n+1}(\kappa R)}{K_n(\kappa R)} \right] \\ & - \kappa r \frac{I_n(\kappa r) K_n(\kappa r) J_n(\alpha r)}{\alpha^2 + \kappa^2} \left[\frac{I_{n+1}(\kappa r)}{I_n(\kappa r)} + \frac{K_{n+1}(\kappa r)}{K_n(\kappa r)} \right], \quad r \neq 0, \end{aligned} \quad (3.1a)$$

$$= \frac{1}{\alpha^2 + \kappa^2}, \quad r = 0, n = 0, \quad (3.1b)$$

$$= 0, \quad r = 0, n \neq 0. \quad (3.1c)$$

Written in this form, the modified Bessel functions appear only as ratios $I_{n+1}(x)/I_n(x)$ and $K_{n+1}(x)/K_n(x)$ or as the products $I_n(x)K_n(x)$ and $I_n(\kappa r)K_n(\kappa R)$. The ratios can be computed directly using standard functional relations, while the products are calculated using the same ratios combined with modified Bessel functions of order zero, which can be computed accurately and stably. Implementation of the solution technique thus requires two elements, a method for the calculation of ratios of modified Bessel functions, and a method for computing the DHT. In practice, the input will not be defined on the nodes of the DHT, so an interpolation scheme will also be required. The method has been coded making use of the GNU Scientific Library (GSL) [4], which provides functions for the computation of scaled versions of the modified Bessel functions, directly returning $I_n(x) \exp[-x]$ and $K_n(x) \exp[x]$. The algorithm has been designed to use these scaled functions, to avoid problems of underflow and overflow.

3.1. Ratios of modified Bessel functions. The ratios of modified Bessel functions can be computed using standard functional relations [7, 8.486]:

$$I_{n-1}(x) = \frac{2n}{x} I_n(x) + I_{n+1}(x), \quad (3.2a)$$

$$K_{n+1}(x) = \frac{2n}{x} K_n(x) + K_{n-1}(x), \quad (3.2b)$$

using an approach similar to that of Amos [1], who writes the ratios of successive functions as:

$$\frac{I_n(x)}{I_{n-1}(x)} = \frac{x}{2n + xI_{n+1}(x)/I_n(x)}, \quad (3.3a)$$

$$\frac{K_{n+1}(x)}{K_n(x)} = \frac{2n}{x} + \frac{K_{n-1}(x)}{K_n(x)}. \quad (3.3b)$$

The recursion for $I_n(x)/I_{n-1}(x)$ is stable for descending n while that for $K_{n+1}(x)/K_n(x)$ is stable for increasing n . The recursion for $K_{n+1}(x)/K_n(x)$ is seeded with $K_1(x)/K_0(x)$, computed using the scaled form of $K_0(x)$ and $K_1(x)$. The recursion for $I_n(x)/I_{n-1}(x)$ is seeded using Olver's asymptotic formula [9, 10.41.10] for modified Bessel functions of large order, as recommended by Amos [1], starting at order equal to the larger of $n + 8$ and 32. The asymptotic expansion is given by:

$$I_n(x) \sim \frac{e^{n\eta}}{(2\pi n)^{1/2}(1+z^2)^{1/4}} \sum_{q=0}^{\infty} \frac{u_q(t)}{n^q}, \quad (3.4)$$

$$z = x/n, \eta = (1+z^2)^{1/2} + \log \frac{z}{1+(1+z^2)^{1/2}}, t = 1/(1+z^2)^{-1/2},$$

$$u_0(t) = 1,$$

$$u_1(t) = (3t - 5t^3)/24,$$

$$u_2(t) = (81t^2 - 462t^4 + 385t^6)/1152,$$

$$u_3(t) = (30375t^3 - 369603t^5 + 765765t^7 - 425425t^9)/414720,$$

while for small arguments, $(x/2)^2 < n + 1$, the series expansion of $I_n(x)$ is used [7, 8.445].

Given a sequence of ratios of modified Bessel functions, the products in Equation 3.1 can be computed as:

$$I_n(\kappa r)K_n(\kappa r) = [I_0(\kappa r)e^{-\kappa r}] [K_0(\kappa r)e^{\kappa r}] \prod_{i=0}^{n-1} \left[\frac{I_{i+1}(\kappa r)}{I_i(\kappa r)} \right] \left[\frac{K_{i+1}(\kappa r)}{K_i(\kappa r)} \right], \quad (3.5)$$

and

$$I_n(\kappa r)K_n(\kappa R) = [I_0(\kappa r)e^{-\kappa r}] [K_0(\kappa R)e^{\kappa R}] \prod_{i=0}^{n-1} A \left[\frac{I_{i+1}(\kappa r)}{I_i(\kappa r)} \right] \left[\frac{K_{i+1}(\kappa R)}{K_i(\kappa R)} \right], \quad (3.6)$$

$$A = e^{\kappa(r-R)/n},$$

where terms of the form $I_n(x) \exp[-x]$ and $K_n(x) \exp[x]$ are computed directly using the scaled form of the modified Bessel functions. The ratios of successive modified Bessel functions are well scaled and multiplying them in pairs as in the products of Equations 3.5 and 3.6 avoids underflow and overflow problems.

3.2. Discrete Hankel Transform. The coefficients of the DHT are computed using the method of Lemoine [8]. This is essentially a quadrature rule based on the zeros of the ordinary Bessel function of order n , $J_n(x)$. The function to be transformed is specified at these zeros x_m , $0 \leq m < M$, $J_n(x_m) = 0$, and the DHT is given by a matrix multiplication of the vector of input data $f(x_m)$ with the matrix entries given

by:

$$B_{mj}^{(n)} = \frac{2}{x_M} \frac{J_n(x_m x_j / x_M)}{|J_{n+1}(x_m) J_{n+1}(x_j)|}. \quad (3.7)$$

In the calculations presented here, the GSL implementation [4] of Lemoine's method was used, but with a modification to compute the zeros of $J_n(x)$ using the $O(M)$ algorithm of Glaser et. al [6].

In order to compute the DHT, the input must be specified at the zeros of the Bessel function. If only one order n is of interest, this presents no difficulties, but if the solution is to be found for multiple values of n , as in solving a Poisson equation, for example, an interpolation scheme is required to transfer the input from the problem mesh onto the DHT nodes, in particular because the zeros are not the same for different orders of Bessel function.

3.3. Interpolation. Given that an interpolation scheme will almost always be needed, the approach used by Pataki and Greengard [11] has been adopted. The domain $0 \leq r \leq R$ is divided into N blocks, $R_n \leq r \leq R_{n+1}$, $n = 0, \dots, N-1$. Each block is discretized with P points, given by the Chebyshev nodes of the second kind:

$$r_{nP+p} = \frac{R_{n+1} + R_n}{2} + \frac{R_{n+1} - R_n}{2} \cos \frac{p\pi}{P}, \quad p = 0, 1, \dots, P. \quad (3.8)$$

Evaluation of $f^{(n)}(r, \kappa)$ within each block is performed using barycentric Lagrangian interpolation [2]. Since Equation 3.1 can be computed directly at arbitrary values of r , the solution is generated on the input nodes, with no requirement for interpolation from the DHT nodes.

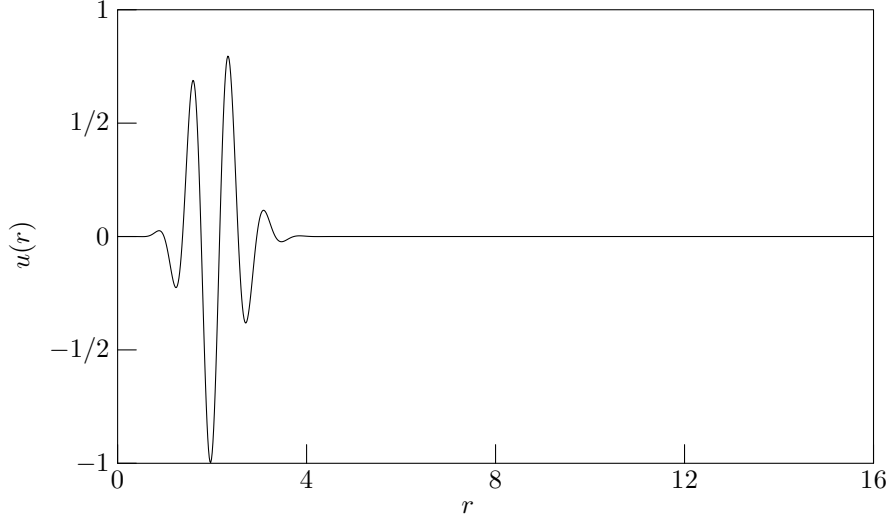
3.4. Summary of algorithm. Given the elements described above, the solution algorithm can be summarized as follows. For a given order n , wavenumber κ and input $f^{(n)}(r, \kappa)$, $0 \leq r \leq R$:

1. generate, if necessary, the DHT matrix and corresponding nodes r_m ;
2. if necessary, interpolate $f^{(n)}(r, \kappa)$ onto the nodes r_m ;
3. perform the DHT to yield $\widehat{f^{(n)}}_m$;
4. evaluate Equation 2.7 at the input nodes using Equations 3.1.

4. Numerical tests. The solution method is tested using a function which can be varied to examine the performance of the algorithm with regard to potential sources of error. The main sources of error in the algorithm arise from the interpolation schemes and aliasing. These errors arise in both the direct method, where the input is specified on the DHT nodes, and when the input must be interpolated from another mesh onto these points.

Interpolation errors arise when the interpolation scheme is unable to accurately resolve the function which is being interpolated. This can occur because the interpolation method proper does not have the required properties to give a well-converged estimate of the underlying function, or because the interpolation nodes are not dense enough to take advantage of an otherwise good interpolation method. In this sense, 'interpolation scheme' refers both to the explicitly stated polynomial interpolation method used to transfer data from the input mesh to the DHT nodes, and to the interpolation which is performed implicitly in the quadrature scheme of the DHT.

The second source of error is aliasing, when the point distribution is not dense enough to capture the spatial frequencies present in the input. This can happen in

FIG. 4.1. Test function with $\alpha = 1$, $\beta = 8$, $m = 8$

the DHT, if the analytically defined input has wavenumbers α_m with $m > M$, so that the expansion of Equation 2.6 does not contain the full set of radial wavenumbers α_m present in the input. Clearly, it can also happen in the Chebyshev interpolation scheme if the node density is not high enough, even if the DHT would otherwise contain enough nodes to capture the full behavior of the input.

In order to assess the performance of the algorithm against these criteria, the test function:

$$u^{(n)}(r) = (r/r_{\max})^m e^{-(r^2 - r_{\max}^2)/\alpha^2} \cos \beta r, \quad m \geq n, \quad (4.1)$$

$$r_{\max} = \alpha(m/2)^{1/2},$$

has been adopted. By varying the parameters α and β , the function can be varied from monotonically decaying, as in Pataki and Greengard's test [11], to oscillatory, Figure 4.1. The r^m term is required for validity of the solution and introducing the terms in r_{\max} scales the amplitude of the cosine on its maximum, so that the maximum amplitude of $u^{(n)}$ is one, reducing errors caused by very large values of r^m .

In testing the algorithm, $\alpha = 1$, $P = 16$, and $R = 16$. The parameters varied were N the number of blocks in r , M the number of DHT nodes, β the frequency of $u^{(n)}$ and κ . The order n was tested up to 64, with $m = n$ in the evaluation of $u^{(n)}(r)$. Tests were conducted for direct solution on the DHT grid, to evaluate the performance of the underlying method, and with interpolation from the Chebyshev nodes. The error measure is the L_∞ norm:

$$\epsilon = \frac{\max |u_c^{(n)}(r, \kappa) - u^{(n)}(r)|}{\max |u^{(n)}(r)|}, \quad (4.2)$$

where $u_c^{(n)}(r, \kappa)$ is the computed solution. For clarity, errors greater than 1 have been set to 1 on the plots.

4.1. Solution on DHT nodes. Figure 4.2 shows the error in the solution when the input is specified directly on DHT nodes, given as a function of the number of

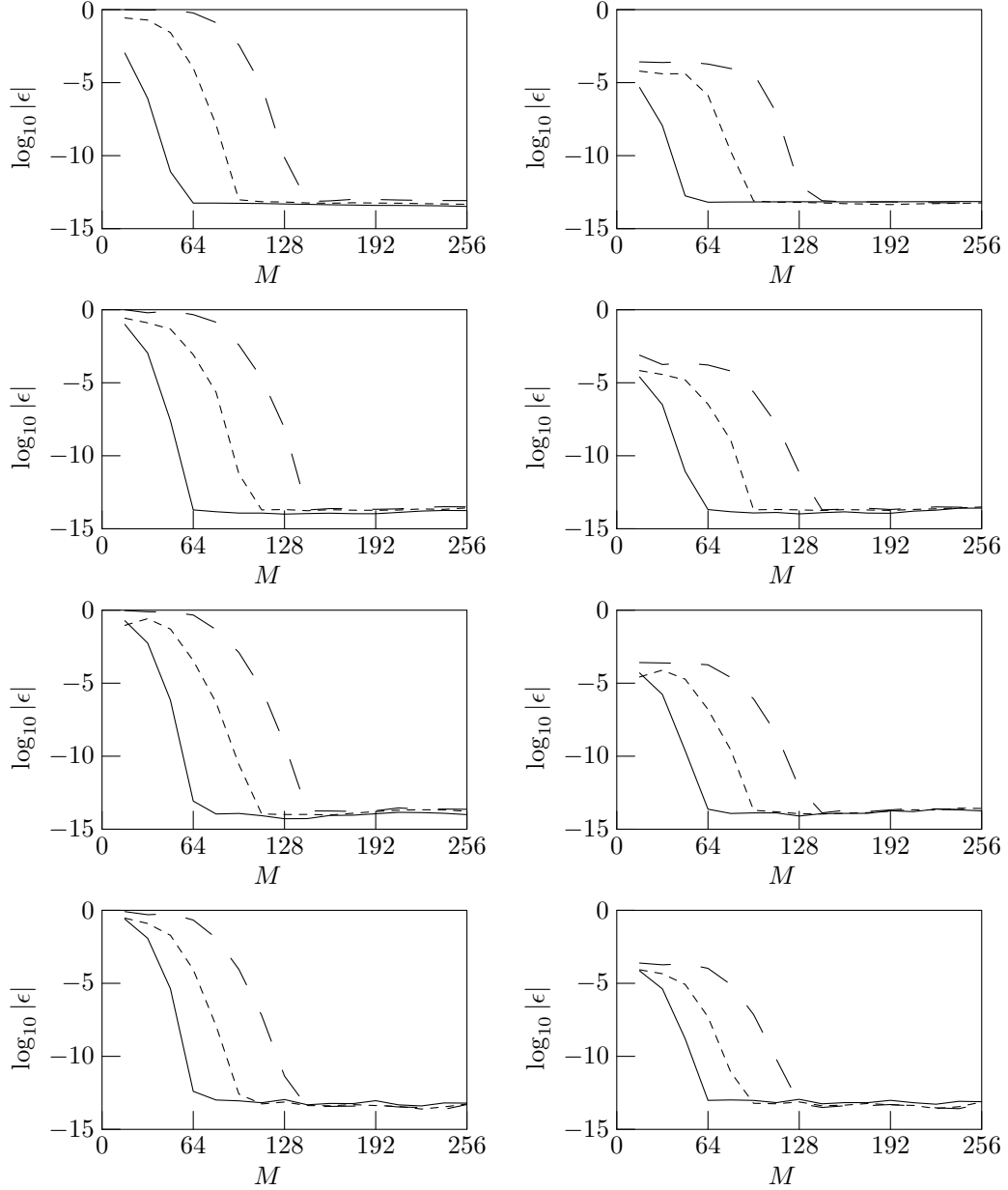


FIG. 4.2. Error in computation on Hankel transform nodes: solid line $\beta = 0$; dashed line $\beta = 8$; long dashed line $\beta = 16$. Left hand column: $\kappa = 16$; right hand column: $\kappa = 1024$. From top to bottom: $n = 0, 16, 32, 64$.

nodes M , for $\beta = 0, 8, 16$, $\kappa = 16, 1024$, and $n = 0, 16, 32, 64$. In each plot, the error behavior is quite similar. For $\beta = 0$, the solution is not oscillatory and there is no aliasing error in the calculation. Thus, the error drops quickly with increasing M , as the node density increases, and reaches a minimum, machine precision, around $M = 64$. In contrast, the error for the oscillatory solutions, $\beta = 8, 16$, remains roughly constant for small node number, before dropping quickly to machine precision. The

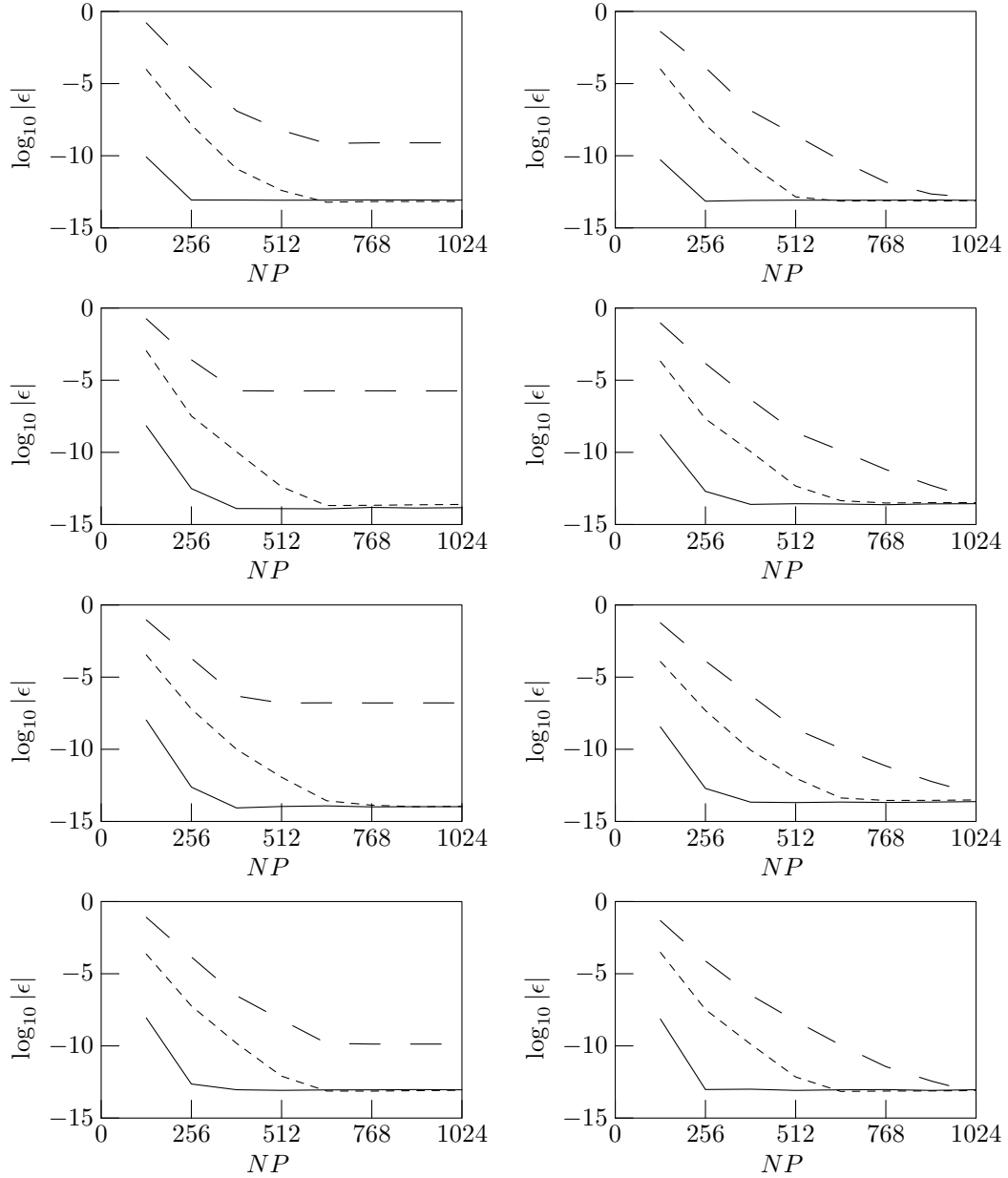


FIG. 4.3. Error in computation on Chebyshev nodes, $\kappa = 1024$: solid line $\beta = 0$; dashed line $\beta = 8$; long dashed line $\beta = 16$. Left hand column: $M = 128$; right hand column: $M = 256$. From top to bottom: $n = 0, 16, 32, 64$.

initial failure of the error to reduce with M can be ascribed to aliasing as there are insufficient points to capture the oscillatory nature of the input, and the reduction in error with M occurs when there is no longer aliasing and the error is controlled by the interpolation method.

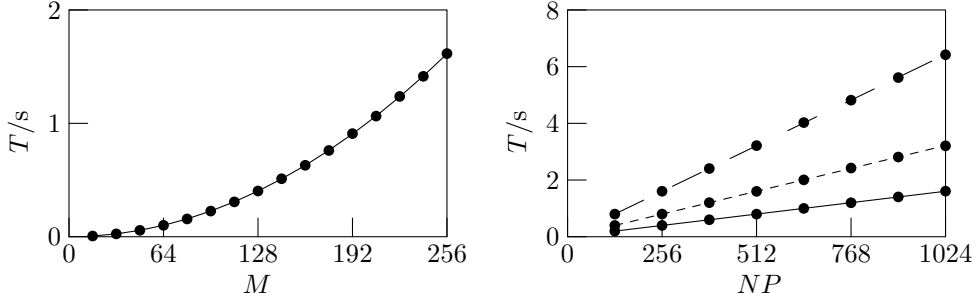


FIG. 4.4. Computation time for solution with $n = 64$, $\kappa = 1024$, $\beta = 16$. Left hand plot uses direct calculation at DHT points; circles: computation time; solid line: M^2 fit. Right hand plot shows computation time for Chebyshev nodes; circles: computation time; curves: linear fit; solid line: $M = 64$; dashed line: $M = 128$; long dashed line $M = 256$.

4.2. Solution on Chebyshev nodes. Figure 4.3 shows similar data, but for the error incurred when interpolating from Chebyshev grids onto the DHT nodes. The parameters varied are the same as in Figure 4.2 but error is now plotted as a function of the number of nodes NP with $M = 128$ and 256 . Referring to Figure 4.2, the choice $M = 128$ gave machine precision accuracy for $\beta = 0$ and $\beta = 8$, though not for $\beta = 16$, while $M = 256$ gave machine precision errors for all three values of β .

Figure 4.3 shows the result of these choices. The left hand column, where $M = 128$ shows the $\beta = 0$ and $\beta = 8$ cases reaching the minimum error, though with the error controlled by NP . As the node density increases, the interpolation scheme reduces the error in the input until the error fixed by the value of M is reached. For $\beta = 16$, the error set by M is greater than machine precision, and the Chebyshev interpolation scheme cannot reduce it below the value reached at $NP \approx 512$. Referring to the right hand column, all three cases show steady reduction in ϵ down to machine precision, but, as might be expected, the $\beta = 16$ case requires more nodes in order to reduce the error to the value set by M .

4.3. Computation time. Finally, Figure 4.4 shows the computational time for the two approaches. The left hand plot shows the time required for direct solution on the DHT nodes, as a function of M . Since the DHT is implemented as a matrix multiplication, the solution time is expected to scale as M^2 and, indeed, the curve fit to the data points shows a computation time $O(M^{2.00})$. In solving on a different set of nodes, such as the Chebyshev points used here, the number of input nodes NP will be greater than M , for reasonable interpolation accuracy. In this case, the computation time can be expected to scale as MNP , i.e. proportional to the number of nodes and to the number of DHT coefficients used in computing the solution at each node. This estimate is borne out by the right hand plot in Figure 4.4 where the fits to the computation time have an exponent equal to 1, to three significant figures, and the slopes of the lines are proportional to M .

5. Conclusions. A method for the solution of a modified Bessel equation which arises in the solution of Poisson's equation in cylindrical geometries has been presented, based on the Hankel transform. Numerical testing has shown the method to be accurate over a wide range of wave numbers and orders. We conclude that for a proper choice of mesh densities and Hankel transform order, the method can achieve machine precision accuracy, for oscillatory and decaying solutions. A sample

implementation of the algorithm, written in C, is available from the author.

6. Acknowledgements. I am grateful to Andras Pataki, Courant Institute, New York University, for helpful discussions on the implementation of his Green's function Poisson solver.

REFERENCES

- [1] D. E. AMOS, *Computation of modified Bessel functions and their ratios*, Mathematics of Computation, 28 (1974), pp. 239–251.
- [2] J.-P. BERRUT AND L. N. TREFETHEN, *Barycentric Lagrange interpolation*, SIAM Review, 46 (2004), pp. 501–517.
- [3] H. CHEN, Y. SU, AND B. D. SHIZGAL, *A direct spectral collocation Poisson solver in polar and cylindrical coordinates*, Journal of Computational Physics, 160 (2000), pp. 453–469.
- [4] M. GALASSI, J. DAVIES, J. THEILER, B. GOUGH, G. JUNGMAN, M. BOOTH, AND F. ROSSI, *GNU Scientific Library Reference Manual*, Network Theory Ltd, Bristol, United Kingdom, 2005.
- [5] L. GENOVESE, T. DEUTSCH, AND S. GOEDECKER, *Efficient and accurate three-dimensional Poisson solver for surface problems*, Journal of Chemical Physics, 127 (2007), p. 054704.
- [6] A. GLASER, X. LIU, AND V. ROKHLIN, *A fast algorithm for the calculation of the roots of special functions*, SIAM Journal on Scientific Computing, 29 (2007), pp. 1420–1438.
- [7] I. GRADSHTEYN AND I. M. RYZHIK, *Table of integrals, series and products*, Academic, London, 5th ed., 1980.
- [8] D. LEMOINE, *The discrete Bessel transform*, Journal of Chemical Physics, 101 (1994), pp. 3936–3944.
- [9] NATIONAL INSTITUTE OF STANDARDS AND TECHNOLOGY, *Digital library of mathematical functions*. <http://dlmf.nist.gov/>, 2010.
- [10] A. PATAKI, personal communication, April 2011.
- [11] A. PATAKI AND L. GREENGARD, *Fast elliptic solvers in cylindrical coordinates and the Coulomb collision operator*, Journal of Computational Physics, 230 (2011), pp. 7840–7852.